



<http://www.diva-portal.org>

Preprint

This is the submitted version of a paper presented at *IEMDC*.

Citation for the original published paper:

Ikram Ul Haq, O., Peretti, L., Hinkkanen, M. (2023)

Estimation of Equivalent Circuit Parameters of Multiphase Induction Machines by Exploitation of Space Harmonic Relations

In: *2023 IEEE International Electric Machines & Drives Conference (IEMDC): San Francisco, CA, USA* IEEE

<https://doi.org/10.1109/IEMDC55163.2023.10238896>

N.B. When citing this work, cite the original published paper.

Permanent link to this version:

<http://urn.kb.se/resolve?urn=urn:nbn:se:kth:diva-337086>

Estimation of Equivalent Circuit Parameters of Multiphase Induction Machines by Exploitation of Space Harmonic Relations

Omer Ikram ul Haq
ABB Corporate Research Center
Västerås, Sweden
omer.ikramulhaq@se.abb.com

Luca Peretti
KTH Royal Institute of Technology
Stockholm, Sweden
lucap@kth.se

Marko Hinkkanen
Aalto University
Espoo, Finland
marko.hinkkanen@aalto.fi

Abstract— A multiphase induction machine model using vector space decomposition or harmonic plane decomposition provides insights into many space harmonics through decoupled reference frames, each hosting specific space vectors related to particular harmonics. The dynamics of each voltage and current space vector are described by an equivalent circuit, whose parameters must be obtained either by finite-element analysis or laboratory measurements. This paper presents and experimentally verifies a methodology for calculating these parameters from a single configuration, with minimal knowledge of the geometrical dimensions of the machine.

Keywords— Electric drives, multiphase, rotating electric machines.

I. INTRODUCTION

Multiphase machines with m number of phases provide m degrees of freedom, which in turn require proper transformations to exploit their full potential. Vector space decomposition (VSD) [1] or harmonic plane decomposition (HPD) [2]–[4] are possible transformations of choice for these types of machines. These transformations decouple the space harmonics into $m/2$ (for even m) or $(m + 1)/2$ (for odd m) vector spaces (i.e. v). Typically, in machines with distributed stator windings, the fundamental vector space $v = 1$ is used for torque generation, while the current in the other vector spaces is regulated to zero [5]. In some cases, the vector spaces can be exploited to estimate parameters in real-time [6]. In other situations, when the stator is not of a distributed winding type, the currents in many vector spaces can produce torque [7]. Recently, it has been demonstrated that suitable current regulation in all vector spaces can change the magnetomotive force pole number [4], [8]. However, achieving all the above requires knowledge of the equivalent circuit parameters for each vector space of the multiphase Induction Machine (IM), which is shown in Fig. 1.

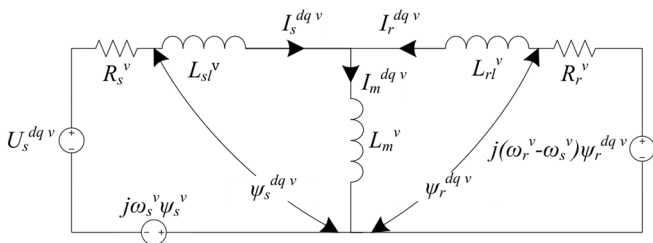


Fig. 1. A T-equivalent circuit of vector space “ v ” in the rotor flux reference frame.

In most literature, lengthy finite-element model (FEM) analyses or extensive experimental measurements are performed to estimate the set of parameters [9], [10]. This paper proposes a simplified methodology for calculating the equivalent circuit parameters of a multiphase IM by exploiting

simple relations between the parameters across multiple vector spaces. Furthermore, in this paper, these estimated parameters are indirectly verified by comparing each vector space's estimated and measured torque. The capability of decomposed vector spaces to produce torque depends on the winding configuration [11]. Thus, looking into common winding configurations of a multiphase IM is vital before calculating the parameters.

II. WINDING CONFIGURATIONS

A multiphase machine's stator can be categorized into two, which are symmetrical winding (SW) configuration and asymmetrical winding (ASW) configuration.

A. Symmetrical Winding Configuration

The SW configuration is the simplest form of phase arrangement where the number of phases is equally distributed along the space defined by the stator. The phase shift between each phase is calculated by $\delta = 2\pi/m$. As an example, 3 and 9-phase SWs are shown in Fig. 2. A drawback of the SW configuration is that it cannot effectively accommodate even numbers of phases. In the case where m is even, the phasors of multiple phases overlap, making them redundant. As an example, 6 and 10-phase SW configurations are shown in Fig. 3, where for the 6-phase SW a is overlapped by $-d$, b is overlapped by $-e$ and so on.

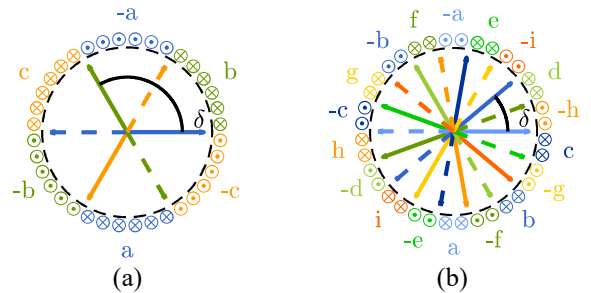


Fig. 2. Phasors of SW configurations accommodating the odd number of phases (a) 3-phase SW, (b) 9-phase SW.

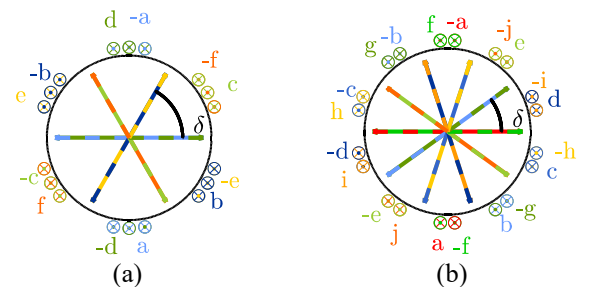


Fig. 3. SW configuration accommodating even number of phases (a) 6-phase SW, (b) 10-phase SW.

B. Asymmetrical Winding configuration

For ASW configurations, the phases can be grouped into asymmetric sets to form a generic solution of the winding configuration that can accommodate both even and odd numbers of phases. An approximate sinusoidal winding distribution is obtained when the phase shift is calculated by

$$\phi = \pi/(Nn) \quad (1)$$

where N is the number of phases in a set and n is the total number of sets. This expression is equivalent to the angle obtained by assuming half-wave symmetry as given in [1]. The total number of phases is defined as $m = Nn$. For example, 6-phase YY30 and 9-phase YY20Y40 ASW configurations are shown in Fig. 4.

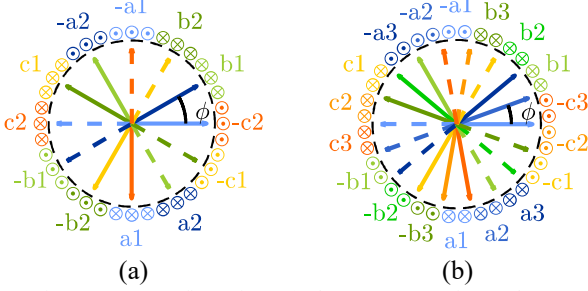


Fig. 4. ASW configuration: (a) phasors representing 6-phase YY30 ASW, (b) phasors representing 9-phase YY20Y40 ASW.

III. MACHINE MODELING

SW and ASW configurations can be modeled using VSD [1]. The applied VSD transformation matrix to each winding configuration in this paper is studied in [11]. It transforms the space vector quantities from the fundamental reference frame (i.e. 123 ref. frame) [1] to the stationary reference frame (i.e. $\alpha\beta$ ref. frame) given by

$$\alpha^v = \frac{2}{m} \sum_{j=0}^{m-1} (x_{N+1} \cos(vj\phi)) \quad v \in \{1,3, \dots, m\}, \quad (2)$$

$$\beta^v = \frac{2}{m} \sum_{j=0}^{m-1} (x_{N+1} \sin(vj\phi)) \quad v \in \{1,3, \dots, m\} \quad (3)$$

Each decomposed vector space v consists of a T-model, as shown previously in Fig. 1. It is assumed that the parameters of each vector space are independent. This condition is met when the machine's magnetic circuit is linear.

IV. T-MODEL PARAMETER ESTIMATION

The T-equivalent circuit parameters describing each multiphase IM vector space and its dynamics are divided into the stator and rotor side parameters. Stator side parameters are: stator resistance R_s , magnetizing inductance L_m and stator leakage inductance L_{sl} . The rotor side parameters are: rotor resistance R_r and rotor leakage inductance L_{rl} . Let us assume, without loss of generality, that the T-equivalent circuit parameters of one of the phase-pole configurations [i.e. base configuration (BC)] could be obtained e.g., with the procedure described in [12]. Our scope is to find the T-equivalent circuit parameters of any other phase-pole combination sharing the same stator and rotor core design, which we call the target configuration (TC). BC and TC refer to the particular use of vector spaces for changing the number of pole pairs in a variable phase-pole IM (i.e. a special case of multiphase machine), which is explained in [4]. The

following section describes the relationship between the parameters across different vector spaces and the number of phases.

A. Stator Resistance

For a wound stator having several strands in a slot, the stator resistance is usually calculated as a DC resistance, i.e.,

$$R_s = \frac{l_c}{\sigma_c a S_c} \quad (4)$$

where σ_c is the specific conductivity of the wire material, a is the number of parallel strands, S_c is the cross-sectional area of the coil, and l_c is the length of the coil given by $2(l_1 + l_{ew})N_s$, where l_1 is the active length, l_{ew} is the end-winding length and N_s is the total number of turns per phase. Assuming the same winding material is used for the BC and TC, the stator resistance of the TC can be calculated by

$$R_s^{TC} = \frac{N_s^{TC}}{N_s^{BC}} \frac{a^{BC}}{a^{TC}} \frac{S_c^{BC}}{S_c^{TC}} R_s^{BC} \quad (5)$$

The quantities with a superscript "TC" belong to the target configuration, while those with a superscript "BC" belong to the base configuration.

B. Magnetizing Inductance

The magnetizing inductance of a machine is given by

$$L_m^{(v)} = m \left(\frac{k_w^{(v)} N_s}{p^{(v)}} \right)^2 \frac{D_\delta^{k_{Lm}}}{\pi \delta_{ef} \mu_o l_1} \quad (6)$$

is explained in Section 3.9 of [13], where D_δ is the air gap diameter, δ_{ef} is the effective air gap, and μ_o is the vacuum permeability. The magnetizing inductance is directly proportional to m , a square of the winding factor for a given vector space $k_w^{(v)}$, and inversely proportional to the square of the number of pole pairs $p^{(v)}$ generated by vector space v . The number of pole pairs generated by a vector space is studied in [11], and it is given by

$$p^{(v)} = vp^{(1)} \quad (7)$$

The rest of the parameters (i.e. k_{Lm}) are constant across all configurations. In order to estimate $L_m^{(v)TC}$, the ratio between $L_m^{(v)TC}$ and $L_m^{(v)BC}$ is calculated. In this paper, the fundamental vector space (i.e. $v = 1$) of BC is used for the calculation of $L_m^{(v)TC}$. Thus, $L_m^{(v)TC}$ having different m , N_s and $p^{(v)}$ is given by

$$L_m^{(v)TC} = \frac{m^{TC}}{m^{BC}} \left(\frac{k_w^{(v)TC} N_s^{TC}}{k_w^{(1)BC} N_s^{BC}} \frac{p^{(1)BC}}{p^{(v)TC}} \right)^2 L_m^{(1)BC} \quad (8)$$

C. Stator Leakage Inductance

The stator leakage inductance consists of multiple components given by (9) and elaborated in Section 4.1 of [13]. The stator leakage inductance can be subdivided into $L_{sl\lambda}$ and L_{slL_m} , where $L_{sl\lambda}$ is proportional to the number of phases m , while L_{slL_m} is a function of the magnetizing inductance and the space harmonic generated by the winding.

$$L_{sl}^{(v)} = \overbrace{L_{u_s} + L_{d_s} + L_{e_{w_s}}}^{L_{sl\lambda}} + \overbrace{L_{s_{q_s}}^{(v)} + L_{\delta}^{(v)}}^{L_{slL_m}} \quad (9)$$

In (9), L_{u_s} is the stator slot leakage inductance given by $\frac{4m}{Q_s} N_s^2 \mu_o l_1 \lambda_{u_s}$ where λ_{u_s} is the permeance factor of the stator

slot and Q_s is the total number of stator slots, L_{d_s} is the stator tooth tip leakage inductance given by $\frac{4m}{Q_s} N_s^2 \mu_0 l_1 \lambda_{d_s}$ where λ_{d_s} is the permeance factor of the stator tooth tip, L_{ew_s} is stator end-winding leakage inductance given by $\frac{4m}{Q_s} q_s N_s^2 \mu_0 l_{ew_s} \lambda_{ew_s}$ where λ_{ew_s} is the permeance factor of the end winding, l_{ew_s} is the total length of end windings, and q_s is the number of stator slots per pole per phase. $L_{sq_s}^{(v)}$ is the stator skewing leakage inductance given by $(1 - k_{sq_s}) L_m^{(v)}$ where k_{sq_s} is the stator skewing factor. Finally, $L_\delta^{(v)}$ is the stator air gap leakage inductance given by $\sigma_\delta L_m^{(v)}$ where the air-gap leakage factor σ_δ is given by

$$\sigma_\delta = \sum_{\substack{h=-\infty \\ h \neq 1}}^{h=\infty} \left(\frac{k_w^{(h)}}{h k_w^{(1)}} \right)^2 \quad (10)$$

σ_δ is the sum of the normalized space harmonics winding factors over the fundamental component. These space harmonics are $h = [5, 7, 11, 13, \dots, \infty]$ for the 3-phase windings, while $h = [11, 13, 23, 25, \dots, \infty]$ and $h = [17, 19, 35, 37, \dots, \infty]$ for 6- and 9-phase windings respectively. Practically, the sum of the first few non-fundamental space harmonics is enough to achieve an acceptable result. Complete detail regarding

To calculate $L_{sl}^{(v)TC}$, the ratio between TC and BC of each part of (9) is calculated. As the permeance factors of each part of $L_{sl\lambda}$ are common among all winding arrangements and are independent of the vector spaces, it is eliminated. Thus, $L_{sl}^{(v)TC}$ is calculated by summing up the partial stator leakage inductances of TC which results in

$$L_{sl}^{(v)TC} = K \left(L_{u_s}^{BC} + L_{d_s}^{BC} + \frac{q_s^{TC}}{q_s^{BC}} L_{ew_s}^{BC} \right) + \mathcal{H} L_m^{(v)TC} \quad (11)$$

where $K = \frac{m^{TC} N_s^{TC^2}}{m^{BC} N_s^{BC^2}}$, and

$$\mathcal{H} = 1 - k_{sq_s}^{TC} + \sum_{\substack{v=-\infty \\ v \neq 1}}^{v=\infty} \left(\frac{k_w^{(v)TC}}{v k_w^{(1)TC}} \right)^2$$

D. Rotor Side Parameters

The rotor side is modeled by two parameters, i.e. L_{rl} and R_r . These parameters can be calculated analytically as given by (12) and (13), following the details of Section 7.1.2 in [13]. The rotor parameters seen from the stator side include the transformer ratio k_{rs} , while L'_{rl} and R'_r are the physical quantities of the rotor that are a function of the pole pairs and vector space v .

$$L_{rl} = \frac{k_{rs}}{Q_r} \left(\frac{N_s k_w^{(v)}}{k_{sq_r}} \right)^2 \left(L'_{rbar} + \frac{L'_{riring}}{2 \sin^2 \left(\frac{v\pi p}{Q_r} \right)} \right) \quad (12)$$

$$R_r = \frac{k_{rs}}{Q_r} \left(\frac{N_s k_w^{(v)}}{k_{sq_r}} \right)^2 \left(R'_{rbar} + \frac{R'_{riring}}{2 \sin^2 \left(\frac{v\pi p}{Q_r} \right)} \right) \quad (13)$$

In (12), (13), Q_r is the total number of rotor bars, k_{sq_r} is the skewing factor of the rotor, L'_{rbar} , R'_{rbar} are the inductance and resistance of a rotor bar, and L'_{riring} , R'_{riring} are the physical inductance and resistance of the rotor ring.

Neglecting the difference between slip frequencies of BC and TC , the winding configurations producing the same number of pole pairs have the same L'_{rl} and R'_r . Thus, the rotor quantities of the TC can be translated from the BC by only knowing k_{rs} of both configurations as given by (14), (15). However, for the calculation of the rotor parameters for a given space harmonic v , the physical inductance and resistance of the bar and ring are required. This information is usually obtained from the FEM analysis of the BC .

$$L_{rl}^{(v)TC} = \frac{m^{TC}}{m^{BC}} \left(\frac{N_s^{TC} k_w^{(v)TC}}{N_s^{BC} k_w^{(v)BC}} \right)^2 L_{rl}^{BC} \quad (14)$$

$$R_r^{(v)TC} = \frac{m^{TC}}{m^{BC}} \left(\frac{N_s^{TC} k_w^{(v)TC}}{N_s^{BC} k_w^{(v)BC}} \right)^2 R_r^{BC} \quad (15)$$

V. TEST MACHINE

A 3-phase, 1-pole-pair IM is used as the BC . The machine's geometry consists of 36 stator slots and 28 rotor bars. The equivalent circuit parameters of the BC are obtained by FEM analysis and are given in TABLE I and TABLE II for stator and rotor side parameters, respectively.

TABLE I. STATOR SIDE PARAMETERS OF THE STANDARD 3-PHASE 1-POLE-PAIR MACHINE (BC)

R_s [mΩ]	L_m [mH]	L_{sl} [mH]	$L_{u_s} + L_{d_s}$ [mH]	L_{ew_s} [mH]	L_δ [mH]
137.33	103.2	1.6	0.43	0.76	0.39

TABLE II. ROTOR SIDE PARAMETERS OF THE STANDARD 3-PHASE 1-POLE-PAIR MACHINE (BC)

L_{rl} [mH]	L'_{rbar} [mH]	L'_{riring} [mH]	R_r [mΩ]	R'_{rbar} [mΩ]	R'_{riring} [mΩ]
2.4	1.51e-3	4.8e-6	156.5	80e-3	0.77e-3

The stator winding of the BC consists of two layers of randomly distributed windings. Each layer contains 10 conductors while both layers are connected in parallel resulting in 10 conductors per slot. Thus, the total number of turns per phase of the BC is given by $N_s^{BC} = 10 \cdot q_s^{BC} = 60$. In order to obtain a reconfigurable winding arrangement, the original winding of the base machine is replaced by an open-end distributed winding consisting of 18 coils with a return path shifted by 180° mechanical degrees, as shown in Fig. 5.

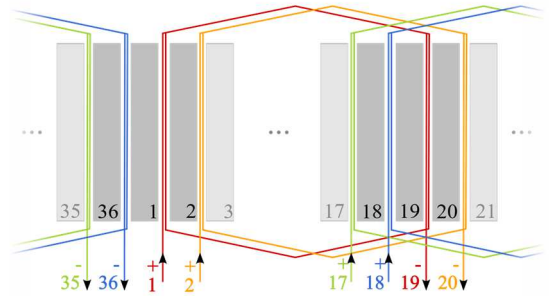


Fig. 5. Coil arrangement of open-end distributed winding of 36 slot stator

This arrangement generates a 1-pole-pair mmf . The phase connections define the + and - signs of the coils. The - sign

is always towards the neutral point of the winding. This type of coil distribution provides the freedom to physically configure the windings into 3, 6, and 9-phase arrangements producing a fundamental magnetic field of 1 pole pair.

A. 6-Phase Configuration

As discussed previously, a 6-phase (or any even number of phases) cannot be optimally arranged in SW configuration. Thus, the test machine is configured as a 6-phase with ASW. The phase arrangement of this machine is shown in Fig. 6, while the coil connections are shown in Fig. 7.

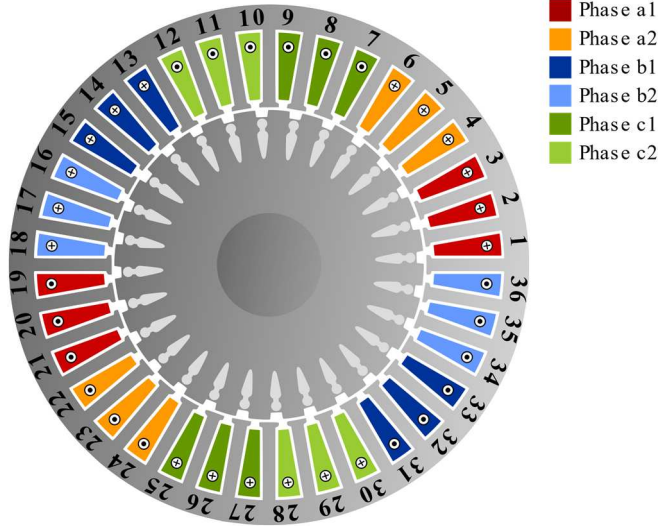


Fig. 6. Open-end distributed winding of 36 slot stator configured in 6-phase ASW configuration.

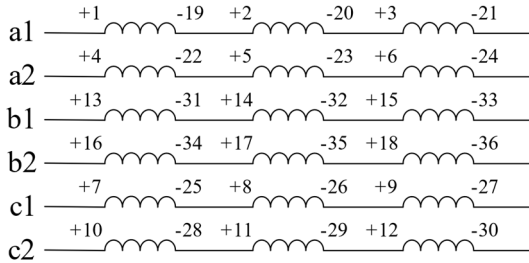


Fig. 7. Coil arrangement of the 6-phase asymmetrical configuration.

This configuration results in 60 turns per phase, i.e., $N_s^6 = 20 \cdot q_s^6 = 60$ turns. Using the parameters defined by BC and the expressions given in Section IV, the parameters of each decomposed vector space are calculated and presented in TABLE III.

TABLE III. ESTIMATED T-EQUIVALENT CIRCUIT PARAMETERS OF A 6-PHASE MACHINE WITH ASW CONFIGURATION

v	1	3	5
R_s [m Ω]	274.7	274.7	274.7
L_m [mH]	221.1	20.8	5.2
L_{sl} [mH]	2.1	1.7	1.7
L_{rl} [mH]	5.2	3.9	2.7
R_r [m Ω]	335.5	214	145.9

According to [11], a 6-phase ASW machine can be decomposed into 3 vector spaces (i.e., 1, 3, and 5). However, in order to excite all the available vector spaces, the neutral point of the winding must be connected to the midpoint of

DC bus i.e. $U_{dc}/2$, which is usually not accessible. In TABLE III the parameters of this non-excitable vector space are written in red color.

B. 9-Phase Configuration

In contrast, a 9-phase machine can be configured as either ASW or SW configurations. For an SW configuration, all decomposed vector spaces except the homopolar space are capable of producing torque without a connection of the neutral point to the midpoint of DC bus [11]. Due to this advantage of SW over ASW configuration, it will be considered for experimental verification. To configure the test machine into a 9-phase machine of either winding configuration, two coils of the test machine are connected in series. These connections give the total number of turns seen by each phase as $N_s^9 = 20 \cdot q_s^9 = 40$. Fig. 8 shows the phase arrangement of a 9-phase SW, and Fig. 9 shows the coil connections.

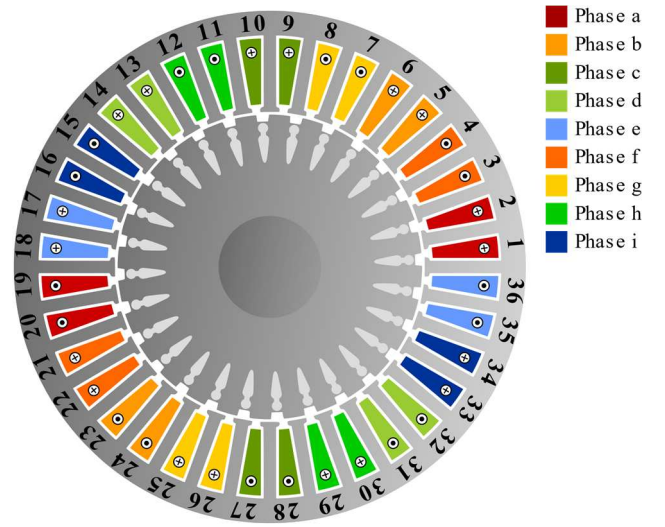


Fig. 8. Open-end distributed winding of 36 slot stator configured in a 9-phase SW configuration.

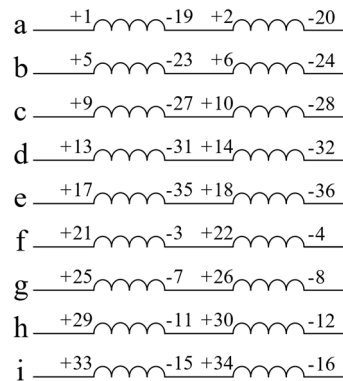


Fig. 9. Coil connections of the open-end distributed winding for the 9-phase symmetrical windings.

The fundamental and higher-order vector space parameters of the 9-phase SW configuration are given in TABLE IV. It can be observed that the inductance L_m of each vector space is significantly reduced for higher-order vector spaces. However, the leakage inductances L_{sl} and L_{rl} remain approximately constant. Due to this phenomenon, the total

leakage magnetic flux of the machine is comparable to the magnetizing flux. This indicates that the performance of higher-order vector spaces will be considerably lower than the fundamental vector space, which will also be verified with the help of laboratory measurements.

TABLE IV. ESTIMATED T-EQUIVALENT CIRCUIT PARAMETERS OF 9-PHASE WINDING CONFIGURATION.

v	1	3	5	7
R_s [m Ω]	183.1	183.1	183.1	183.1
L_m [mH]	149.3	15.6	4.9	2.1
L_{sl} [mH]	1.2	0.9	0.9	0.9
L_{rl} [mH]	3.5	2.9	2.5	2.1
R_r [m Ω]	226.5	160.5	137.6	111.6

VI. EXPERIMENTAL SETUP

The multiphase experimental test setup shown in Fig. 10 consists of four 3-phase converters (i.e., C1, C2, C3, and C4) controlled by an Opal-RT OP5700 system. These converters have a common DC-link voltage powered by a 22-kW regenerative load drive (ABB ACS880). The load drive also controls a 15-kW 3-phase 1-pole-pair IM which is mechanically coupled to the test machine. The test machine is configured as a 9-phase machine in SW configuration to validate the methodology, leaving C4 open. Furthermore, the OP5700 is interfaced with a 1000-pulse encoder and a torque transducer to measure rotor speed and output torque.

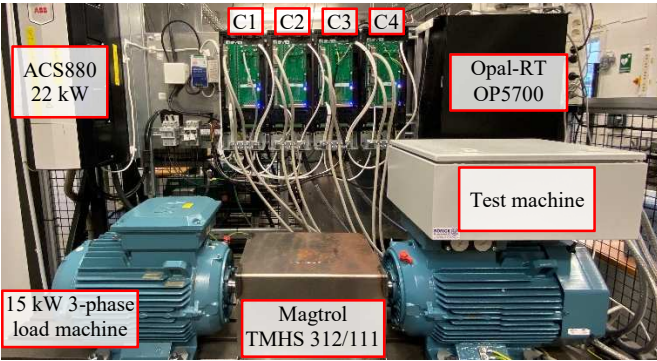


Fig. 10. Coil connections of the open-end distributed winding for the 9-phase symmetrical windings.

A. Parameter Verification

In order to verify the accuracy of the calculated parameters and the performance accuracy, the torque production of each vector space is experimentally verified. A simple vector control of each vector space of the 9-phase test machine is implemented. The block diagram of this vector control is shown in Fig. 11. The vector control of each vector space is oriented along its respective rotor flux reference frame. This reference frame is obtained by a basic current model explained in [14] and shown in Fig. 12.

Each vector control block takes the rotor flux $\psi_r^{(v)}$ and torque $\tau_e^{(v)}$ as a reference which is denoted by the superscript *. Based on these references, a voltage vector rotating at an independent stator frequency i.e. $\omega_s^{(v)}$ is generated for each vector space. These voltage vectors are transformed back to 9-phase references using VSD transform. The current model is implemented using the inverse-Gamma model and is defined by (16) and (17). Thus, the T-model parameters must be converted to inverse-Gamma parameters given in [15].

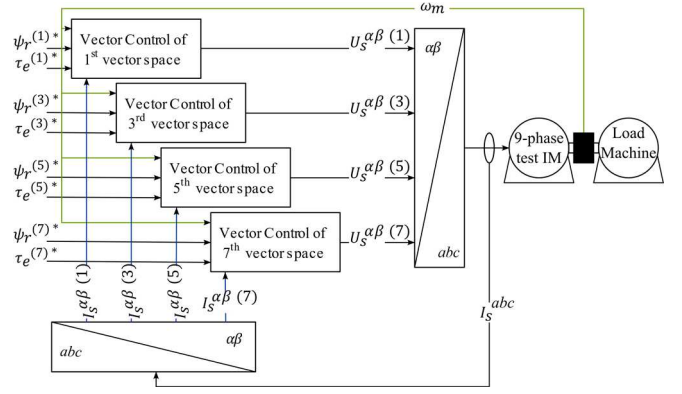


Fig. 11. Implemented vector control of a 9-phase machine configured as SW.

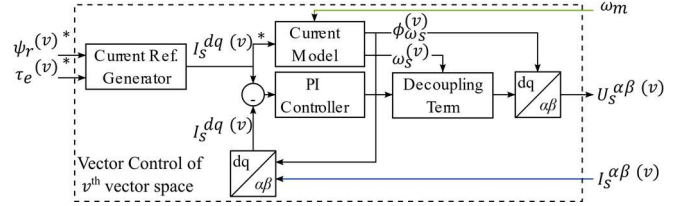


Fig. 12. Vector control of v^{th} vector space.

$$\omega_s^{(v)} = \frac{\omega_r^{(v)}}{v_x p^{(1)}} \omega_m - \frac{\omega_{sl}^{(v)}}{I_s^q(v) R_r^{(v)}} \quad (16)$$

$$\phi_{\omega_s}^{(v)} = \int \omega_s^{(v)} dt \quad (17)$$

In this paper, the cross-coupling between the vector spaces is neglected. Each vector space is excited individually to avoid the impact of the cross-coupling. During the measurements, the $\psi_r^{(v)*}$ of each vector space is set and kept constant for the whole torque reference range of the active vector space. These $\psi_r^{(v)*}$ values are given in TABLE V, together with the resultant $I_s^d(v)$.

TABLE V. ROTOR FLUX REFERENCE AND THE RESULTANT CURRENT

v_x	1	3	5	7
$\psi_r^{v_x*}$ [Vs]	0.6	0.19	0.1	0.06
$I_s^{d v_x*}$ [A]	4	12	20	28

Fig. 13 shows the comparison between $\tau_e^{(v)*}$ and measured $\tau_e^{(v)}$ as a function of current magnitude which is given by

$$|I_s^{(v)}| = \sqrt{(I_s^d(v))^2 + (I_s^q(v))^2}. \quad (18)$$

The minimum current of each vector space is defined by the $\psi_r^{(v)*}$ which is calculated as $|I_s^{(v) \min}| = \psi_r^{(v)*} / L_m^{(v)}$.

The measured torques of the fundamental vector space follow the reference with some discrepancies. There are multiple causes for this discrepancy. A few of these are related to the missing models of the skin effect and the longer end-windings inherited due to the open end-winding design. To calculate the skin-effect factor, knowledge about the rotor bar dimensions is required, which is usually not readily available. Due to this reason, skin effect is neglected during

R_r calculation. Thus, the calculated R_r is only valid for low slips regions which is usually acceptable for most applications.

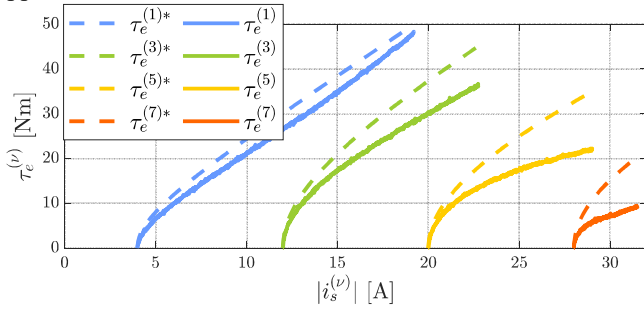


Fig. 13. Comparison between reference and measured torque as a function of the current magnitude.

Furthermore, the proposed methodology provides constant parameters while neglecting the impact of magnetic saturation. Thus at higher currents, the saturation of the stator and rotor core introduces errors between $\tau_e^{(v)*}$ and $\tau_e^{(v)}$. Finally, the BC is used as a reference, and errors between calculated and physical quantities are scaled for higher-order vector spaces. Due to this fact, the error between the reference and measured torque is significant for higher-order vector spaces. This is one of the drawbacks of this methodology.

VII. CONCLUSION

The paper proposes and evaluates a methodology for translating the T-equivalent circuit parameters of a known IM into the T-equivalent parameters of a target IM having different winding configurations but sharing a common stator and rotor core design. The methodology is applied to an open-end winding IM, which can be physically configured into a 3-phase, 6-phase, or 9-phase topology. This multiphase machine topology is modeled using VSD, which decomposes the space harmonics into multiple vector spaces. Furthermore, independent T-equivalent circuits can represent these vector spaces. The 9-phase SW configuration is chosen for experimental verification as all of its decomposed vector spaces can produce torque. The accuracy of calculated parameters and performance of each vector space is verified by employing a closed-loop vector control.

It is observed that the magnetizing inductance of each vector space of the 9-phase configuration reduces significantly while the total leakage inductances remain approximately constant. Furthermore, these obtained parameters are valid for linear regions where magnetic saturation can be neglected. Due to the scaling factor of magnetizing inductance, the discrepancies between calculated and physical parameter is also scaled, resulting in slightly wrong parameter estimation and nonlinear torque production. Due to this phenomenon, higher-order vector spaces' performance is worse than the fundamental vector space.

It is concluded that the proposed methodology provides sufficiently accurate parameters for the magnetically linear regions of the machine. However, for more precise parameter estimation of each vector space, FEM analysis is

recommended. Finally, in order to improve the performance of higher-order vector spaces, the geometry of the stator and rotor must be optimized.

REFERENCES

- [1] A. A. Rockhill and T. A. Lipo, "A generalized transformation methodology for polyphase electric machines and networks," in *2015 IEEE International Electric Machines & Drives Conference (IEMDC)*, Coeur d'Alene, ID, May 2015, pp. 27–34. doi: 10.1109/IEMDC.2015.7409032.
- [2] Y. Wu, G. F. Olson, L. Peretti, and O. Wallmark, "Harmonic Plane Decomposition: An Extension of the Vector-Space Decomposition - Part I," in *IECON 2020 The 46th Annual Conference of the IEEE Industrial Electronics Society*, Singapore, Singapore, Oct. 2020, pp. 985–990. doi: 10.1109/IECON43393.2020.9255228.
- [3] G. F. Olson, Y. Wu, L. Peretti, and O. Wallmark, "Harmonic Plane Decomposition: An Extension of the Vector-Space Decomposition - Part II," in *IECON 2020 The 46th Annual Conference of the IEEE Industrial Electronics Society*, Singapore, Singapore, Oct. 2020, pp. 991–996. doi: 10.1109/IECON43393.2020.9254279.
- [4] Y. Wu, G. F. Olson, and L. Peretti, "Pole-Transition Control of Variable-Pole Machines Using Harmonic-Plane Decomposition," *IEEE Trans. Ind. Electron.*, vol. 69, no. 1, pp. 1–8, 2022, doi: 10.1109/TIE.2022.3231328.
- [5] Yifan Zhao and T. A. Lipo, "Space vector PWM control of dual three-phase induction machine using vector space decomposition," *IEEE Trans. Ind. Appl.*, vol. 31, no. 5, pp. 1100–1109, Oct. 1995, doi: 10.1109/28.464525.
- [6] Z. Li, G. Feng, C. Lai, J. Tian, W. Li, and N. C. Kar, "Dual DC current injection-based stator winding temperature tracking for dual three-phase permanent magnet synchronous machine using Kalman filter," *IET Electr. Power Appl.*, vol. 13, no. 11, pp. 1726–1733, Nov. 2019, doi: 10.1049/iet-epa.2019.0049.
- [7] K. Wang, Z. Y. Gu, Z. Q. Zhu, and Z. Z. Wu, "Optimum Injected Harmonics Into Magnet Shape in Multiphase Surface-Mounted PM Machine for Maximum Output Torque," *IEEE Trans. Ind. Electron.*, vol. 64, no. 6, pp. 4434–4443, Jun. 2017, doi: 10.1109/TIE.2017.2669888.
- [8] M. Osama and T. A. Lipo, "Modeling and analysis of a wide-speed-range induction motor drive based on electronic pole changing," *IEEE Trans. Ind. Appl.*, vol. 33, no. 5, pp. 1177–1184, Oct. 1997, doi: 10.1109/28.633794.
- [9] H. S. Che, A. S. Abdel-Khalik, O. Dordevic, and E. Levi, "Parameter Estimation of Asymmetrical Six-Phase Induction Machines Using Modified Standard Tests," *IEEE Trans. Ind. Electron.*, vol. 64, no. 8, pp. 6075–6085, Aug. 2017, doi: 10.1109/TIE.2017.2677349.
- [10] Y. Wu, A. Pisani, G. Falk Olson, K. Bitsi, O. Wallmark, and L. Peretti, "FEM-based Parameter Estimation for a Variable Phase-Pole Induction Machine," in *2021 23rd European Conference on Power Electronics and Applications*, Ghent, Belgium.
- [11] O. Ikram ul Haq, L. Peretti, S. G. Bosga, and R. S. Kanchan, "Online Winding Reconfiguration of a Multiphase Stator," presented at the 14th IEEE International Conference on Power Electronics and Drive Systems (PEDS 2023), Montreal, Canada, Aug. 2023. unpublished
- [12] A. G. Yepes *et al.*, "Parameter Identification of Multiphase Induction Machines With Distributed Windings—Part 1: Sinusoidal Excitation Methods," *IEEE Trans. Energy Convers.*, vol. 27, no. 4, pp. 1056–1066, Dec. 2012, doi: 10.1109/TEC.2012.2220967.
- [13] J. Pyrhönen, T. Jokinen, and V. Hrabovcová, *Design of Rotating Electrical Machines: Pyrhönen/Design*. Chichester, UK: John Wiley & Sons Ltd, 2013. doi: 10.1002/9781118701591.
- [14] P. L. Jansen and R. D. Lorenz, "A physically insightful approach to the design and accuracy assessment of flux observers for field oriented induction machine drives," *IEEE Trans. Ind. Appl.*, vol. 30, no. 1, pp. 101–110, Feb. 1994, doi: 10.1109/28.273627.
- [15] G. R. Slemon, "Modelling of induction machines for electric drives," *IEEE Trans. Ind. Appl.*, vol. 25, no. 6, pp. 1126–1131, Dec. 1989, doi: 10.1109/28.44251.